IOP Publishing Plasma Sources Science and Technology

Plasma Sources Sci. Technol. **23** (2014) 065049 (11pp) doi:10.1088/0963-0252/23/6/065049

# Radio-frequency capacitively coupled plasmas in hydrogen excited by tailored voltage waveforms: comparison of simulations with experiments

**P Diomede[1], D J Economou[1], T Lafleur[2,3], J-P Booth[2] and S Longo[4]**

[1] Plasma Processing Laboratory, Department of Chemical & Biomolecular Engineering, University of Houston, Houston, TX 77204-4004, USA
[2] Laboratoire de Physique des Plasmas, CNRS, Sorbonne Universités, UPMC Univ Paris 06, Univ Paris-Sud, Ecole Polytechnique, 91128 Palaiseau, France
[3] ONERA-The French Aerospace Lab, 91120 Palaiseau, France
[4] Dipartimento di Chimica, Universita' degli Studi di Bari, via Orabona 4, 70126 Bari, Italy

E-mail: padiomede@gmail.com and Economou@uh.edu

Received 28 August 2014
Accepted for publication 2 October 2014
Published 11 November 2014

**Abstract**

A combined computational–experimental study was performed of a geometrically symmetric capacitively coupled plasma in hydrogen sustained by tailored voltage waveforms consisting of the sum of up to three harmonics. Predictions of a particle-in-cell with Monte Carlo collisions/fluid hybrid model were in reasonably good agreement compared to data from an array of experimental plasma diagnostics. The plasma was electrically asymmetric, with a dc self-bias developed, for all but a sinusoidal voltage waveform. Hydrogen ions ($H^+$, $H_2^+$, $H_3^+$) bombarding the electrodes exhibited different ion flux-distribution functions due to their different masses and collisionality in the sheath. Plasma density, ion flux and absolute value of the dc self-bias all increased with increasing the number of harmonics. The energy of ions bombarding the substrate electrode may be controlled by switching the applied voltage waveform from (positive) 'peaks' to (negative) 'valleys'.

Keywords: capacitively coupled plasmas, tailored voltage waveforms, hydrogen plasmas

(Some figures may appear in colour only in the online journal)

## 1. Introduction

Capacitively coupled plasma (CCP) reactors are widely used in plasma processing. In particular, for large area plasma enhanced chemical vapour deposition (PECVD), the parallel plate reactors employed are necessarily nearly symmetric, i.e. the area of the radio frequency (RF) powered electrode is nearly the same as that of the grounded electrode. In such systems, the deposition rate can be increased by increasing the RF power but, for plasma excitation using a classical sinusoidal voltage, the concomitant increase in ion energy can degrade the quality of the deposited film [1]. Under these conditions, the sheath voltage on both electrodes (hence the ion bombardment energy (IBE)), is almost the same. One way to break the link between power and IBE is to exploit the so-called electrical asymmetry effect (EAE) [2]. This is based on the application of a dual frequency voltage, comprising of fundamental plus second harmonic, by which it is possible to shift the majority of the time-averaged voltage from one sheath to the other, simply by adjusting the relative phase between the two signals. This opens the possibility of moving the majority of the high-energy ion bombardment away from the substrate, without affecting the ion flux [2]. Moreover, Wang and Wendt [3] demonstrated that the ion energy distribution on a substrate, in contact with an independently powered high density plasma, can be controlled by applying tailored voltage waveforms (TVWs) to the substrate holder. Nearly mono-energetic ion energy distribution functions were obtained by manipulating

 

the applied waveform such that the sheath voltage over the substrate was at a constant negative value with intermitted sharp positive voltage peaks to neutralize the total current reaching the electrode over a cycle. This allowed the energy of ions bombarding the substrate to be above the threshold for $SiO_2$ ion-stimulated etching, but below the threshold for Si etching, in fluorocarbon plasmas, thereby enabling extremely high selectivity of $SiO_2$ over Si. Johnson *et al* [4] combined the two approaches to excite a CCP reactor with trapezoidal voltage waveforms comprised of a sum of harmonics, thus allowing separate control of the plasma density (which in turn controls the flux of reactive neutrals and ions) and energy of ions bombarding the substrate.

Several studies followed to investigate the physics behind this kind of TVWs. Measurements of IBE [5] showed the effect of increasing the number of harmonics and confirmed particle-in-cell with Monte Carlo collisions (PIC-MCC) simulation predictions that, for a given peak-to-peak voltage ($V_{pp}$), when the number of harmonics is increased, the IBE on one of the electrodes remains low and fairly constant, whereas on the other electrode the IBE increases [6]. The same authors, also showed that the plasma density does not change when the polarity of the TVW is inverted (from positive 'peaks' to negative 'valleys') [6] and that, increasing the number of harmonics leads to a higher electron density, ion flux and power deposition in the discharge [7]. In [8] a detailed experimental characterization of a CCP discharge was performed and results were compared to a PIC-MCC simulation. All these studies were performed in Ar. However, the gas mixtures used in PECVD usually contain molecular gases, e.g. $H_2/SiH_4$ to deposit silicon thin films for the manufacture of photovoltaic solar cells, where actually hydrogen is the majority component.

Previous studies of the EAE in molecular gases have been performed in $CF_4$ [9] and oxygen [10], but were only based on PIC-MCC simulation and analytical models. In [11] a limited comparison with experiments in an oxygen CCP was also performed, but the ion flux-distribution functions (IF-DFs) were not analysed. In [12] the effect of dust on electron heating and dc self-bias in hydrogen-diluted silane discharges was studied by means of optical and electrical diagnostics and an analytical model. In [13] a simulation study was presented of the field reversal in electrically asymmetric CCPs in hydrogen and hydrogen containing discharges using a hybrid plasma equipment model. In [14], the same hybrid model was used to investigate flux-energy distribution functions of $H_3^+$ ions which were compared with experimental data and an analytical model. In addition, the EAE on photovoltaic cell performance [15] and the effect of TVWs on the nucleation and growth mechanisms [16] in the deposition of microcrystalline silicon using $SiH_4/H_2$ plasmas was studied experimentally.

In view of the above, a better understanding of $H_2$ containing plasmas excited by different TVWs is desirable. Since $H_2$ is the most abundant component used as a diluent, pure $H_2$ plasma dynamics is to be investigated first. Preliminary results by Longo and Diomede [17] have shown that the EAE produces different effects for different ion species in $H_2$ plasmas. In particular, the behaviour of the $H_2^+$ ion may differ markedly from that of $H_3^+$ and $H^+$. This is due to differences in the relevant ion–neutral processes affecting the transport of these species in the bulk plasma as well as the sheath, for example the fact that the primary ions $H_2^+$ are rapidly converted to $H_3^+$ by collisions with $H_2$.

In the present work, an array of experimental results in a hydrogen CCP are compared with PIC-MCC simulations. Measured quantities include electron density, dc self-bias, IBE, ion flux and IF-DFs for three different ions, namely $H_3^+$, $H_2^+$ and $H^+$. Also, quantities that were not measured experimentally, but are important from the materials processing point of view are shown and discussed.

## 2. Simulations

A hydrogen plasma in a geometrically symmetric parallel plate CCP reactor was simulated using a hybrid model described in [18, 19] with additional features reported in [20]. It was a one-dimensional simulation that self-consistently coupled a PIC-MCC description for charged species (electrons, $H^+$, $H_2^+$, $H_3^+$ and $H^-$), with a reaction–diffusion fluid model for neutrals (14 vibrational levels of the electronic ground state of $H_2$, and H atoms). The chemical reactions in the gas phase and on the surface were those reported in tables 1 and 2 of [19]. Reactions included electron elastic scattering, vibrational excitation and deactivation, electronic excitation, dissociation, ionization, dissociative attachment, ionic conversions, ion–neutral charge exchange, detachment, ion neutralization, vibrational–vibrational and vibrational–translational energy exchanges, vibrational deactivation and atom recombination on surfaces, as well as secondary electron emission by ion bombardment.

In order to simulate a discharge powered by TVWs, new boundary conditions were implemented for the solution of Poisson's equation. Since the discharge was capacitively coupled, the period-average charge through the circuit must be zero. The total charge imbalance $Q$ was updated at every time step by counting the charged particles striking the two electrodes, taking into account the particle charge, the differential weight (used to improve the statistics of minority species [18]), and any secondary electron emission. Then, the voltage on the powered electrode $V(t)$ was calculated using the applied voltage $V_a(t)$, and the blocking capacitor voltage, $V(t) = V_a(t) - Q/C$, assuming a capacitance $C = 10\,\text{nF}$. The other electrode was assumed to be grounded. Moreover, the previously used cross section for the momentum transfer collisions between $H_3^+$ and $H_2$ molecules by Simko [21], was replaced by the one in [22], the latter giving a closer agreement with the experiments for the $H_3^+$ ion flux-distribution functions. Electrons reaching the walls were assumed to be fully absorbed.

The equations of motion for the charged particles were integrated by using the leap-frog method and the electric field was calculated by solving the Poisson equation, with the space charge obtained by using a first-order particle-grid interpolation. The field solver and the particle/Monte Carlo solver were coupled matching the fixed PIC time step $\Delta t$ with the values of the times between collisions using the *modified time step* approach [23]. About 100 000 particles were used

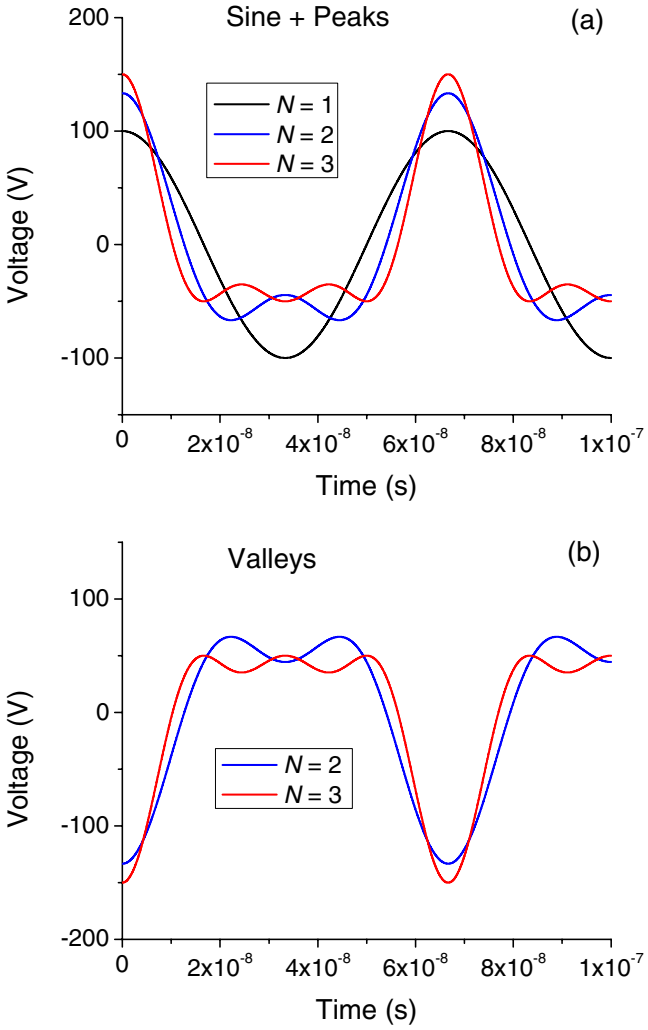


**Figure 1.** Sine along with 'peaks' (*a*) and 'valleys' (*b*) waveforms with $N = 1, 2$ and 3.

in the simulations, with 400 grid points, and a time step of $\sim 10^{-11}$ s, in order to satisfy accuracy/stability criteria [24]. Simulations were executed until steady-state was reached, which typically took about 1000 RF cycles.

The applied voltage was a sum of $N$ harmonics [8], according to the formula:

$$V_a(t) = \sum_{r=1}^{N} V_r \cos(2\pi r f t + \theta_r), \quad V_r = V_{pp} \frac{2(N - r + 1)}{(1 + N)^2},$$

where $V_{pp}$ is the peak-to-peak voltage. The amplitude of each harmonic, $V_r$, was devised to have a $V_{pp}$ independent of the number of harmonics $N$. 'Peaks' voltage waveforms were obtained by setting $\theta_r$ equal to zero, whereas 'valleys' waveforms were obtained by setting $\theta_r$ equal to $\pi$ for all harmonics. The fundamental frequency $f$ ($N = 1$) of the applied voltage was 15 MHz, $V_{pp}$ was set to 200 V, and the number $N$ of harmonics was varied from 1 to 3 (figure 1). At higher harmonics the RF generator used in the experiments could not deliver a $V_{pp}$ beyond 140 V without significant waveform distortion, because there was no matching network (due to the use of multiple frequencies), and most of the applied power was reflected back to the generator.

## 3. Experiments

Experiments were performed in the DRACULA CCP plasma reactor [8]. The reactor was cylindrically symmetric with aluminum electrodes having a diameter of 50 cm, and separated by a distance of 2.5 cm. The bottom electrode was powered, while the top electrode was grounded. The plasma between the electrodes was radially bounded by the combination of a large Pyrex cylinder and a thick Teflon dielectric. In this way the plasma 'saw' almost equal electrode areas. The chamber was pumped with a turbomolecular pump backed by a mechanical pump. Pressure was measured using ion and baratron gauges. Hydrogen gas was injected into the reactor via a side port in the chamber, and the flow rate was adjusted using a mass flow controller.

The powered electrode was connected to a class A, broadband, RF power amplifier via a 4.5 nF bias capacitor. The amplifier was controlled using a function generator and PC with a LabVIEW program that created and sent the desired voltage waveforms. The frequency response of the reactor and the plasma impedance in general distorted this waveform, so a Fourier transform feedback technique [8, 25] was used to ensure that the desired waveforms could be produced on the powered electrode. Placed between the powered electrode and the bias capacitor was a SOLAYL voltage–current probe (described in detail in [26]) that was used to monitor the discharge current and power. The discharge voltage and dc self-bias were measured with a 100 : 1 high-voltage probe directly connected to the powered electrode.

The plasma density was measured with a floating hairpin probe that was placed in the reactor through an additional side port. The probe was located between the electrodes in the centre of the reactor, and consisted of a 50 mm long, 0.125 mm diameter, tungsten wire with hairpin ends separated by about 3–4 mm. The presence of the sheath around the hairpin was compensated for by using the method described in [27].

Embedded in the grounded electrode was an array of 16 ion flux probes each having a diameter of 6 mm, and lying on a single diametric line across the electrode. The probes were biased to a negative voltage between −20 and −40 V to repel electrons. The ion current was then found by extrapolation to zero bias, so as to correct for the effect of sheath expansion around the probes.

Ion flux-energy distribution functions (IF-DFs) were measured with a HIDEN EQP mass spectrometer with energy analyser. The spectrometer entrance orifice was embedded in the grounded electrode and was aligned with the axis of the reactor. Because of the need to accurately know the ion energy dependent transmission function (which requires trajectory simulations) [28, 29], the focusing electrodes were turned off and only ions in a narrow acceptance half-angle of about 2° were measured.

## 4. Results and discussion

For both simulations and experiments, the interelectrode gap was 2.5 cm, and the gas pressure was set at 150 mTorr. The gas temperature was assumed to be 300 K, since the pressure used

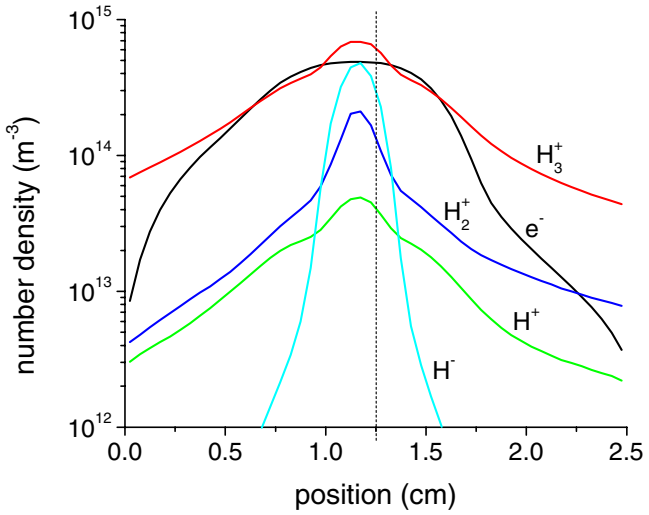


**Figure 2.** Time-average charged particle number densities as a function of position across the discharge gap for the case of 'valleys' waveform with $N = 3$.

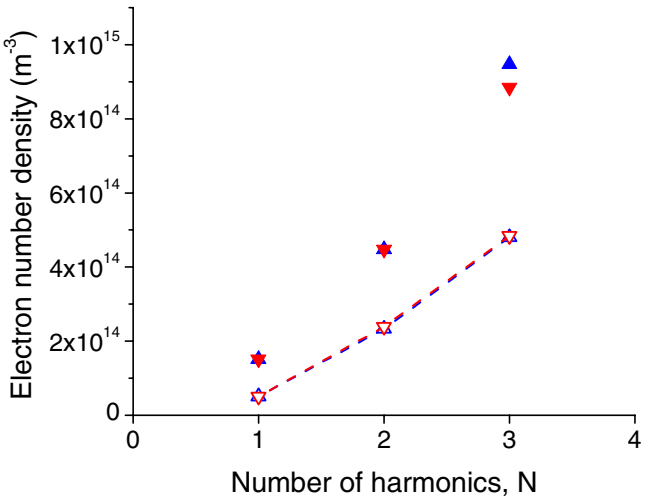


**Figure 3.** Electron number density at the mid-plane of the reactor as a function of the number of harmonics. Blue upwards pointing triangles and red downwards pointing triangles represent results for 'peaks' and 'valleys' waveforms, respectively; solid symbols refer to experiments, open symbols to simulations.

is high, 150 mTorr, and the measured plasma densities are very low, so that collisional heating is expected to be negligible. Figure 2 shows the time-average charged particle number density as a function of position across the interelectrode gap, for 'valleys' waveform, with $N = 3$ harmonics. The left electrode was powered while the right electrode was grounded. For the 'peaks' waveform, each spatial density distribution was the mirror image, with respect to the mid-plane of the discharge (at $x = 1.25$ cm), of the corresponding distribution shown in figure 2. The EAE in hydrogen was simulated in [17], where it was found that negative ions, which concentrate near the maximum of the plasma potential, were off centre, and that the electron and $H_2^+$ ion profiles were strongly asymmetric in the two sheaths. Analogous results were found with the present calculations. The shape of the electron density profile in the sheaths shown in figure 2 is similar to the one obtained for Ar at 75 mTorr with $N = 2$ harmonics [6]. One can also see that $H_3^+$ is the dominant positive ion with $H_2^+$ and $H^+$ having far lower densities. The H-atom number density maximum varied from $4.6 \times 10^{17}$ m$^{-3}$ for the sine waveform ($N = 1$) to $1.1 \times 10^{18}$ m$^{-3}$ for the 'peaks'/'valleys' waveforms with three harmonics, yielding a maximum degree of dissociation of about 1–2 $\times 10^{-4}$. Negative ions are produced by dissociative attachment of vibrational states of molecular hydrogen and pile up near the center of the discharge at the maximum of the plasma potential.

For the figures below, the following legends were adopted: Blue upwards pointing triangles and red downwards pointing triangles represent results for 'peaks' and 'valleys' waveforms, respectively; solid symbols refer to experiments, open symbols to simulations. For the IF-DF figures 6–11, black, blue and red lines indicate results for waveforms with $N = 1$, $N = 2$ and $N = 3$, respectively.

In figure 3 the electron density at the mid-plane of the reactor is shown. The electron density increases with the number of harmonics as in Ar [8]. While the simulation results do not depend on which waveform ('peaks' or 'valleys') was used, as expected due to the geometrical symmetry of the reactor, the experiments show a small difference for $N = 3$. This may be due to waveform distortion, which is exacerbated for the higher harmonics. The simulation underestimates the measured electron density by a factor of ∼2. Comparison of results for the deposited power (not shown) gave similar discrepancy between simulation and experiment. Such discrepancy may be attributed to the omission in the model of some process producing electrons, or the use of cross-sections that are not accurately known. The simulation has underestimated the experimental plasma density before [18]. Underestimation of the electron density was also found for the same type of waveforms in Ar [8] for the case of four and five harmonics. Another reason for the underestimation of the electron density could be that, in finding the electron density from the hairpin probes, a common model [27] to compensate for the sheath around the hairpin wires was used. This model starts losing validity at very low densities where the sheath is large, and so the difference between experimental and simulation densities could also be influenced by this; i.e. the model might over-compensate the experimental electron densities.

In figure 4 results for the ion current density are shown. Measurements were done with a planar probe located on the surface of the grounded electrode. This sensor 'sees' all positive ion species at all incidence angles. However, the ion flux probes cannot distinguish between ions and secondary electrons due to ion bombardment, so the secondary electron current was taken into account in the simulation, with a probability of secondary electron emission by ion impact of 0.1. Following the trend of the electron number density, the ion current density increases with the number of harmonics as well. While the simulation shows a difference in the ion current density between the 'peaks' and the 'valleys' waveforms, the experimental results seem to not be influenced by the shape of the waveform. This is in contrast to what was previously found in an Ar CCP for a peak-to-peak voltage of 100 V [8], where higher values for the ion flux for the 'valleys' waveforms were found at pressures greater than 7 Pa.

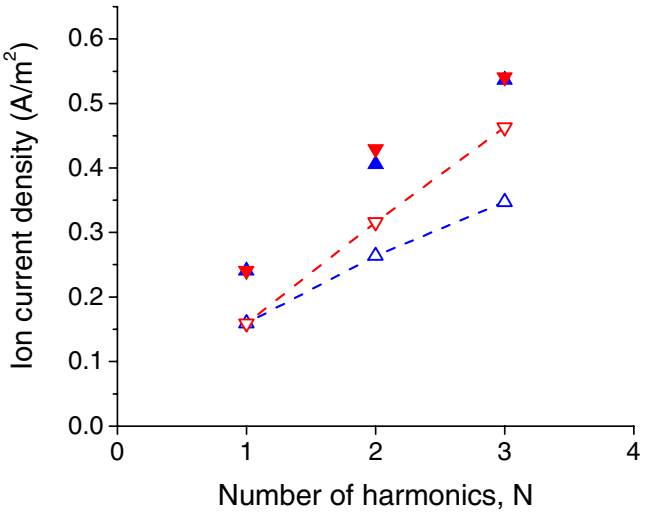


**Figure 4.** Ion current density to the grounded electrode as a function of the number of harmonics. Symbols as in figure 3.

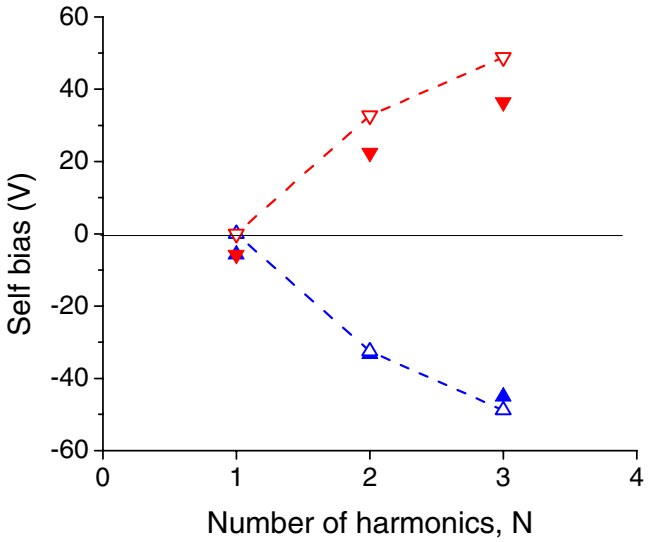


**Figure 5.** Self-bias as a function of the number of harmonics. Symbols as in figure 3.

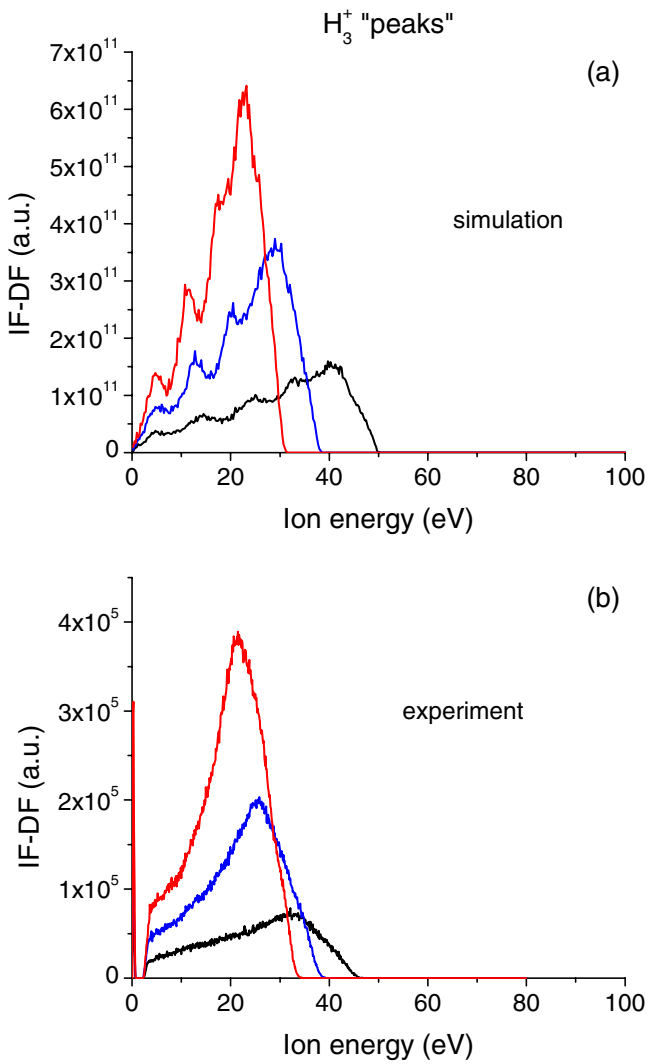


**Figure 6.** IF-DFs restricted to ions within 2° half-angle with respect to the normal on the grounded electrode for the $H_3^+$ ions and 'peaks' waveform for different number of harmonics: (*a*) simulation and (*b*) experiment; black line, $N = 1$; blue line, $N = 2$; red line, $N = 3$.

Figure 5 displays results for the dc self-bias. In the experiments, there is a small residual geometric self-bias of −5.8 V for the sine waveform, which increases the absolute value of the biases and ion energies for the 'peaks' waveforms, while reducing the biases and ion energies for the valleys waveforms. There is very good agreement between simulation and experiment for the dc self-bias voltage. This is despite the disagreement in electron density because, as shown by an analytical sheath model for CCPs excited by arbitrary waveforms [30], and in [31], the self-bias does not depend on the absolute values of the electron density, but only on the voltage waveform and ratio of the average ion densities in the two sheaths. For the hydrogen discharge, the agreement for the self-bias is better for the 'peaks' than for the 'valleys' waveforms, while the opposite is true for the Ar discharge for up to three harmonics [8].

The IF-DFs for each of the three ions, for both the 'peaks' and 'valleys' waveforms, and up to three harmonics are shown in figures 6–11. The mass spectrometer used for experimental work does not measure the ion energy distribution function, but rather the ion velocity distribution function in the forward direction (in energy units). As stated above, for the measurements shown in the present work all focusing electrodes of the mass spectrometer were turned off, resulting in an effective ion acceptance half-angle of about 2°. This was done to avoid corruption of the measurements due to energy-dependent acceptance angle of the spectrometer when focusing is used. This also applies to the ratio of fluxes of each species. The narrow acceptance angle was taken into consideration in the simulation when sampling ions impacting the electrodes to calculate the distributions and the ratio of fluxes. Also, there is a very low ion energy (∼0.2 eV) spike in the experimental distribution function data that is an artefact of the spectrometer. Furthermore, in the experiments, apart from this initial spike no ions are detected at energies below about 2.5 eV, again an artefact of the instrument. As shown in figure 3, the experimental plasma density is higher than the simulated

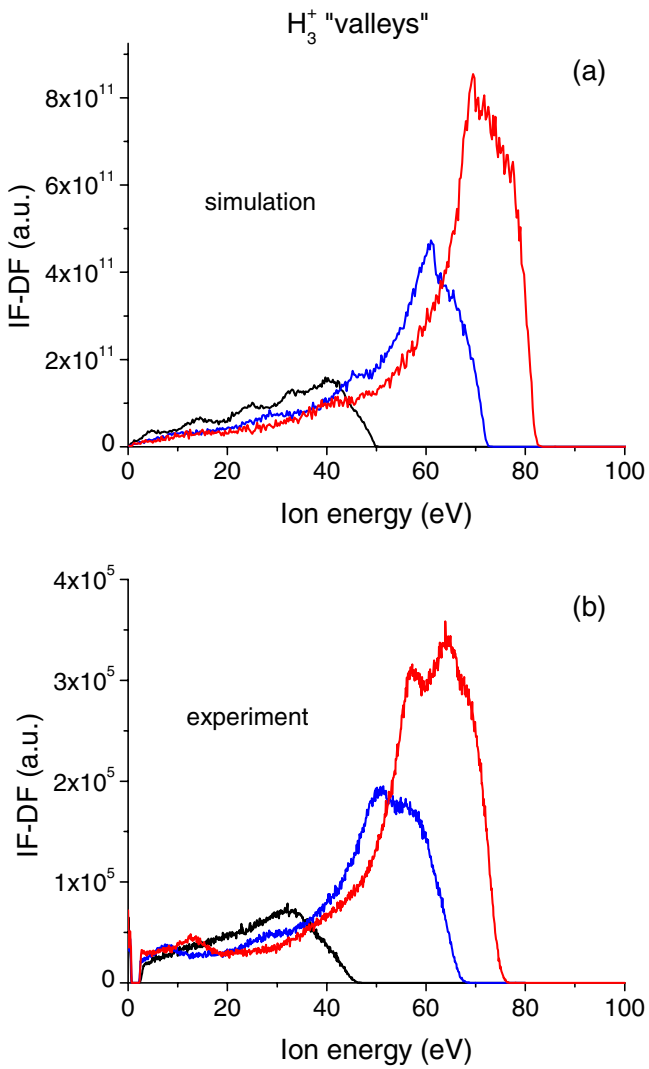


**Figure 7.** IF-DFs restricted to ions within 2° half-angle with respect to the normal on the grounded electrode for the $H_3^+$ ions and 'valleys' waveform for different number of harmonics: (*a*) simulation and (*b*) experiment; black line, $N = 1$; blue line, $N = 2$; red line, $N = 3$.

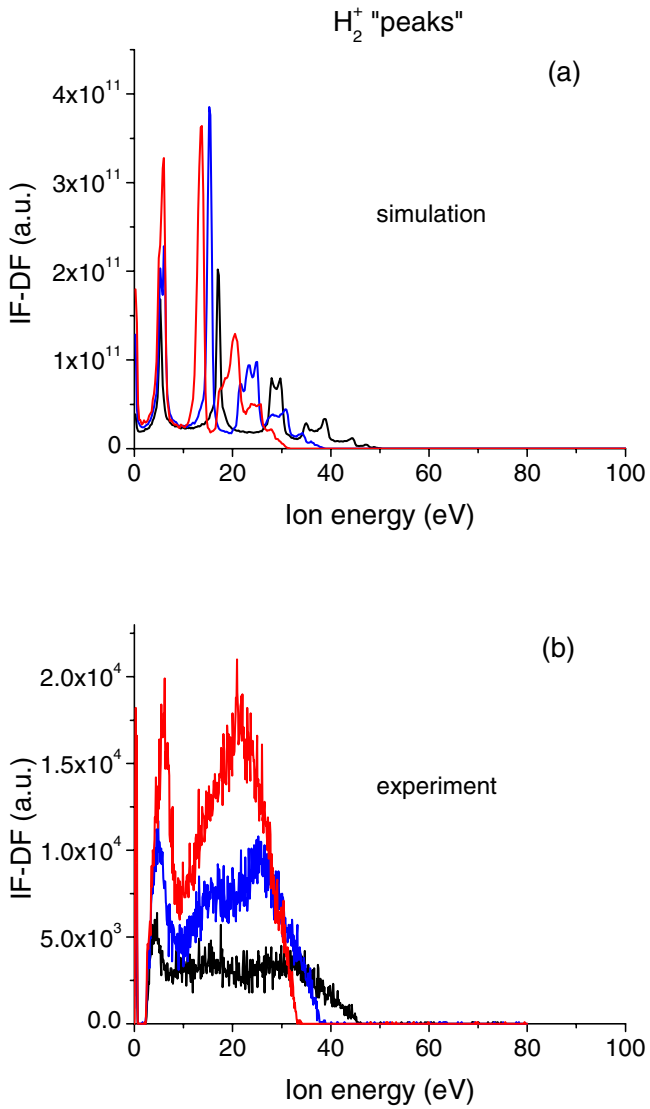


**Figure 8.** IF-DFs restricted to ions within 2° half-angle with respect to the normal on the grounded electrode for the $H_2^+$ ions and 'peaks' waveform for different number of harmonics: (*a*) simulation and (*b*) experiment; black line, $N = 1$; blue line, $N = 2$; red line, $N = 3$.

one, therefore larger sheaths and hence higher chances of ion collisions in the sheath are expected for the simulation. Finally, the noise in the experimental measurements increases considerably for the minority ions $H_2^+$ and $H^+$.

There is good agreement between simulation and experiment regarding the overall shape of the IF-DFs of the dominant ($H_3^+$) ions as a function of the number of harmonics, for both the 'peaks' (figure 6) and the 'valleys' (figure 7) waveforms. However, the simulation predicts secondary peaks due to the higher ion collisionality in the sheaths. As the number of harmonics increases, the distributions shift towards lower energies for the 'peaks' waveform, and towards higher energies for the 'valleys' waveform. This is true for all three ions and reflects the trends of the average and maximum IBE (figures 13 and 14). This is also related to the trend of the dc self-bias with the number of harmonics (figure 5). A similar trend for the ion distribution functions with the number of harmonics was found for Ar [8]. The agreement between simulation and experiment for the $H_2^+$ ions (figures 8 and 9) is not as good as for $H_3^+$, but nevertheless the trend and the shape of the high-energy peaks for different number of harmonics are captured by the simulation. The simulation predicts additional peaks at lower energies due to the larger sheath width of the simulation and thus higher probability to create $H_2^+$ by symmetric charge-exchange collisions in more locations in the sheath [32, 33]. The experimental IF-DFs for the $H^+$ ions (figures 10 and 11) are very similar to those for the $H_3^+$ ions, apart from the noise, and this is consistent with the results for the average and maximum IBE shown in figures 13 and 14. The simulation results are somewhat different from the experiments, but again this can be attributed to the larger sheath width that leads to higher ion collision probability, hence to more secondary low-energy peaks.

In figure 12 the average IBE as a function of the number of harmonics is shown for the $H_3^+$, $H_2^+$ and $H^+$ ions. The agreement between simulation and experiment is good for all ions. In general, the IBE is lower for the 'peaks' waveforms than for

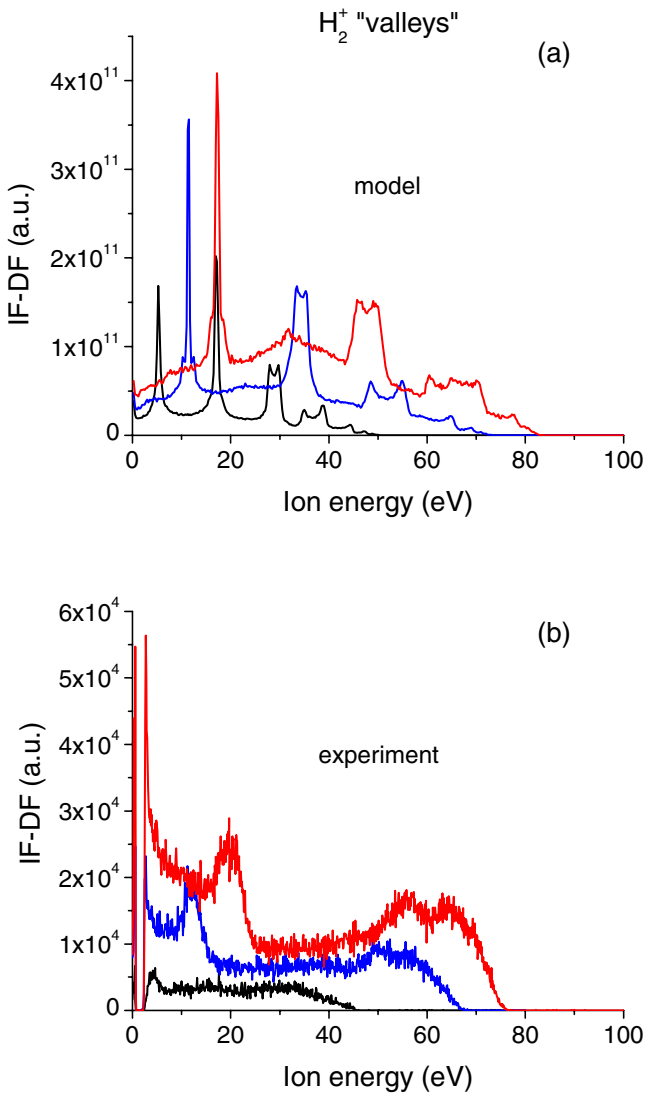


**Figure 9.** IF-DFs restricted to ions within 2° half-angle with respect to the normal on the grounded electrode for the $H_2^+$ ions and 'valleys' waveform for different number of harmonics: (*a*) simulation and (*b*) experiment; black line, $N = 1$; blue line, $N = 2$; red line, $N = 3$.

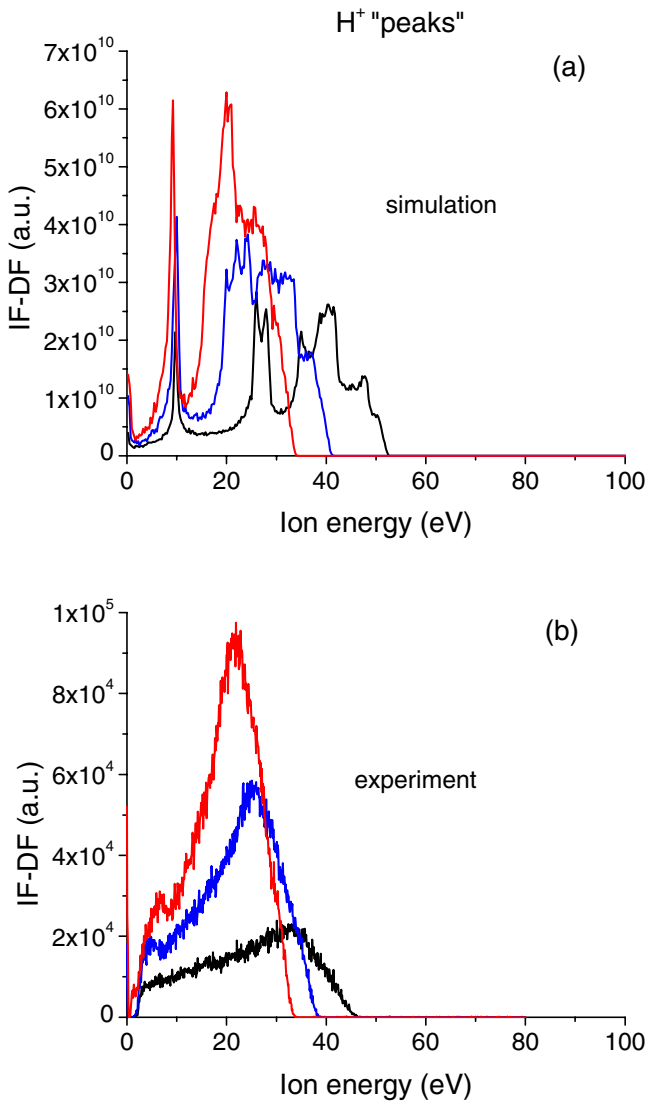


**Figure 10.** IF-DFs restricted to ions within 2° half-angle with respect to the normal on the grounded electrode for the $H^+$ ions and 'peaks' waveform for different number of harmonics: (*a*) simulation and (*b*) experiment; black line, $N = 1$; blue line, $N = 2$; red line, $N = 3$.

the 'valleys' waveforms. For the 'peaks' waveforms there is a decrease of the IBE with the number of harmonics. This differs from the findings in an Ar CCP [8], where the average IBE did not change much for the peaks waveforms. For the 'valleys' waveforms there was an increase in IBE with the number of harmonics in [8], as found in the present work. In [8], the constant IBE for the 'peaks' waveforms was attributed to the opposing effects of the reduced collisionality of ions as the sheath width decreased with the increase of the plasma density, that led to an increase of the IBE and the concurrent decrease in the sheath voltage, that led to a decrease of the IBE. However, though the plasma density in the discharge centre increases in a similar way for both 'peaks' and 'valleys' waveforms, the sheath voltage increases for the 'valleys' but decreases for the 'peaks' [6]. For the hydrogen discharge, the reduced ion collisionality does not compensate for the decrease in the sheath voltage for the 'peaks' waveforms. For the 'valleys' waveforms, the reduced collisionality in the sheath due to the decrease of the sheath width, and the higher sheath voltage result in an increase of the IBE. Also $H_3^+$ and $H^+$ appear to be on average more energetic than $H_2^+$ and have similar trends of the average IBE with the number of harmonics. The lower energy of $H_2^+$ ions can be explained by more ion–neutral collisions due to the fact that the cross section for symmetric charge exchange ($\sim 10^{-19}$ m$^2$ for the $H_2^+$–$H_2$ pair) is much higher than the total cross section for the other two positive ions.

The maximum IBE for each ion is shown in figure 13. The trend and the values versus number of harmonics are very similar for the three ions, with a higher maximum IBE for the 'valleys' waveforms compared to the peaks waveforms, both in experiments and in simulation. The maximum IBE follows the trend of dc self-bias, taking into account the residual geometrical asymmetry of the reactor (figure 5). For the average IBE values reported in figure 12, the acceptance angle of the mass spectrometer was taken into account in the simulation, while results for the maximum IBE were

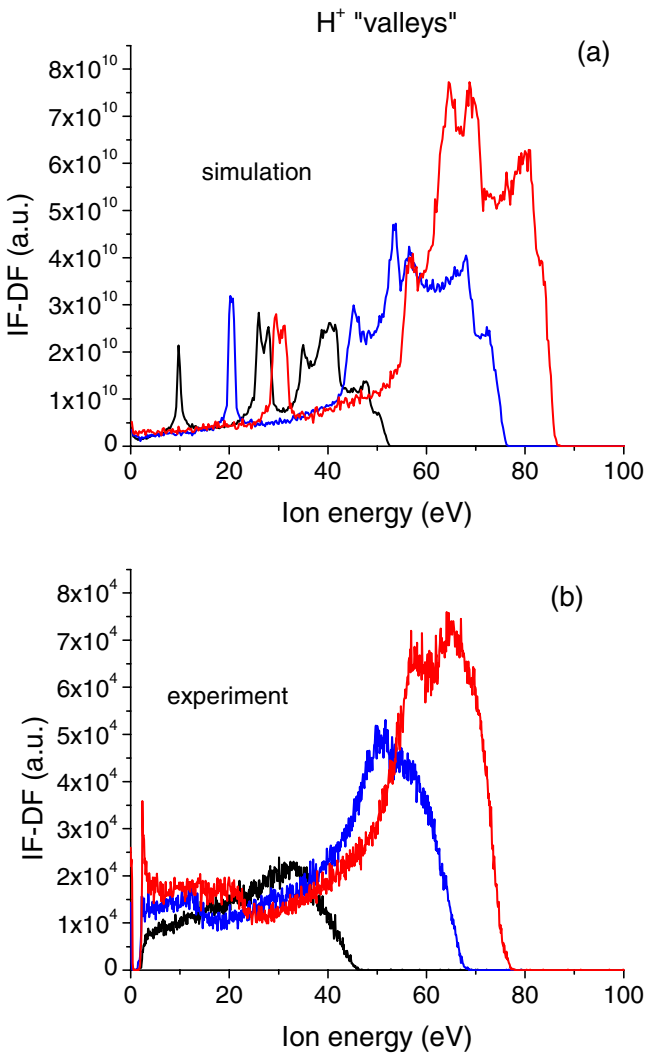


**Figure 11.** IF-DFs restricted to ions within 2° half-angle with respect to the normal on the grounded electrode for the $H^+$ ions and 'valleys' waveform for different number of harmonics: (*a*) simulation and (*b*) experiment; black line, $N = 1$; blue line, $N = 2$; red line, $N = 3$.

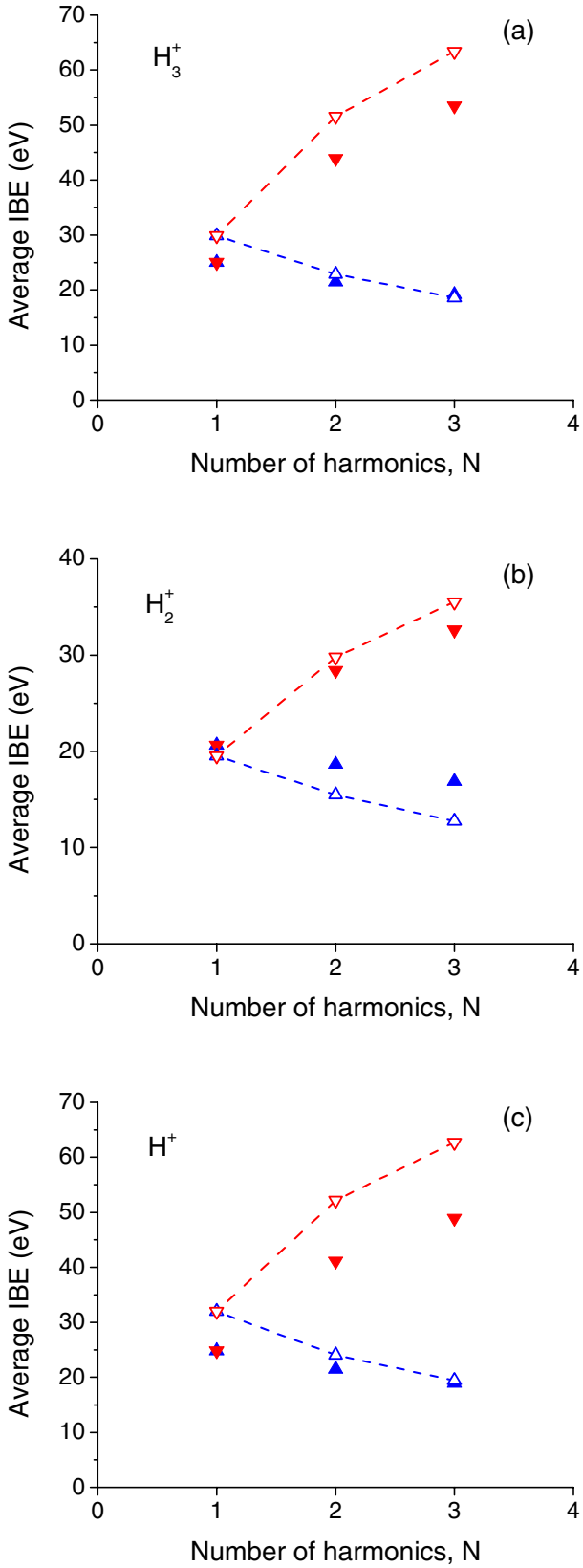


**Figure 12.** Average IBE to the grounded electrode as a function of the number of harmonics for the $H_3^+$ (*a*), $H_2^+$ (*b*) and $H^+$ (*c*) ions. The experimental acceptance half-angle (2°) of the mass spectrometer was taken into account in the simulation. Blue upwards pointing triangles and red downwards pointing triangles represent results for 'peaks' and 'valleys' waveforms, respectively; solid symbols refer to experiments, open symbols to simulations.

not affected by the acceptance angle. Overall, the trends of maximum IBE with the number of harmonics are similar to those found in Ar [8].

Figure 14 shows the ratio of the ion current density to the grounded electrode for 'valleys' waveforms to that for 'peaks' waveforms for each of the three ions. Both simulation and experiment show the ratio to increase with the number of harmonics. For three harmonics the simulation predicts a higher increase for $H_3^+$ and $H^+$, but again the disagreement with the experiment for three harmonics can be attributed to waveform distortion, as previously discussed. The agreement between simulation and experiment for the $H_2^+$ ion is very good.

In figure 15, simulated IF-DFs (including ions impacting on the surface at all angles) are shown for $H_3^+$ for one, two and three harmonics. The complete IF-DFs are important in materials processing applications, because ions may impact the surface with a wide angular distribution. The main difference with figures 6 and 7, where only ions within the acceptance angle were considered, is that the low-energy tail

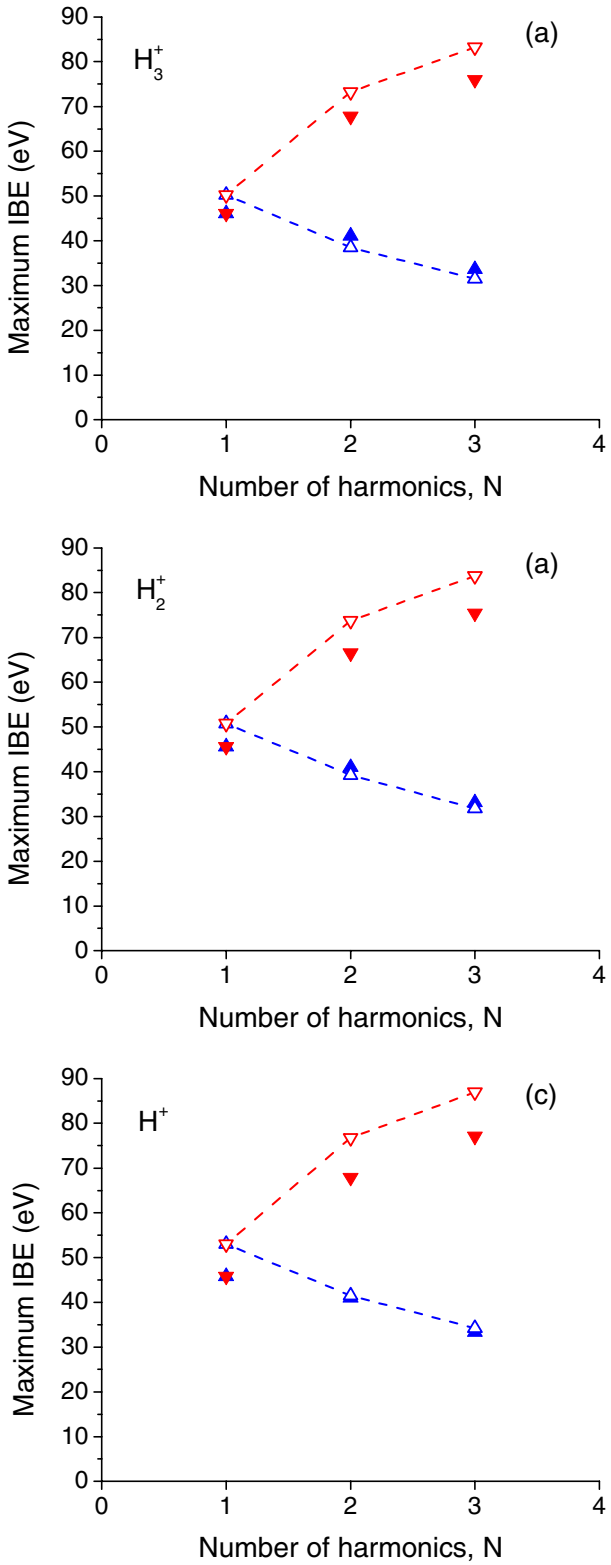


**Figure 13.** Maximum IBE to the grounded electrode as a function of the number of harmonics for the $H_3^+$ (*a*), $H_2^+$ (*b*) and $H^+$ (*c*) ions. The experimental acceptance angle (2°) of the mass spectrometer did not affect the simulation results. Symbols as in figure 12.

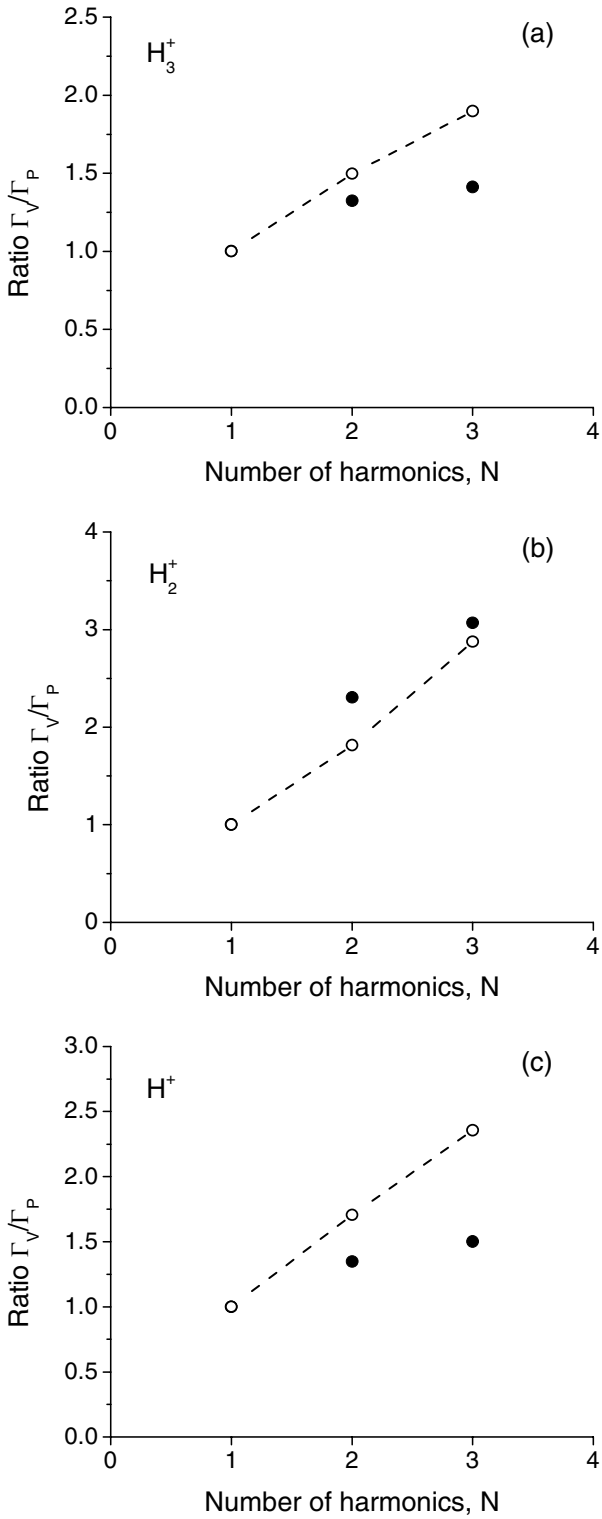


**Figure 14.** Ratio of the ion current density to the grounded electrode for 'valleys' waveforms relative to 'peaks' waveforms as a function of the number of harmonics for the $H_3^+$ (*a*), $H_2^+$ (*b*) and $H^+$ (*c*) ions. The experimental acceptance half-angle (2°) of the mass spectrometer was taken into account in the simulation. Solid circles refer to experiments, open circles to simulations.

is enhanced. This is because low-energy ions generally have a bigger angular spread compared to high-energy ions. Thus, low-energy ions do not fall within the very narrow acceptance angle of the instrument. This is also confirmed by the fact that the high-energy part of the distributions did not change appreciably, whether or not the acceptance angle was included. The expected bimodal structure, resulting from ions entering the sheath in different phases of the RF cycle, experiencing

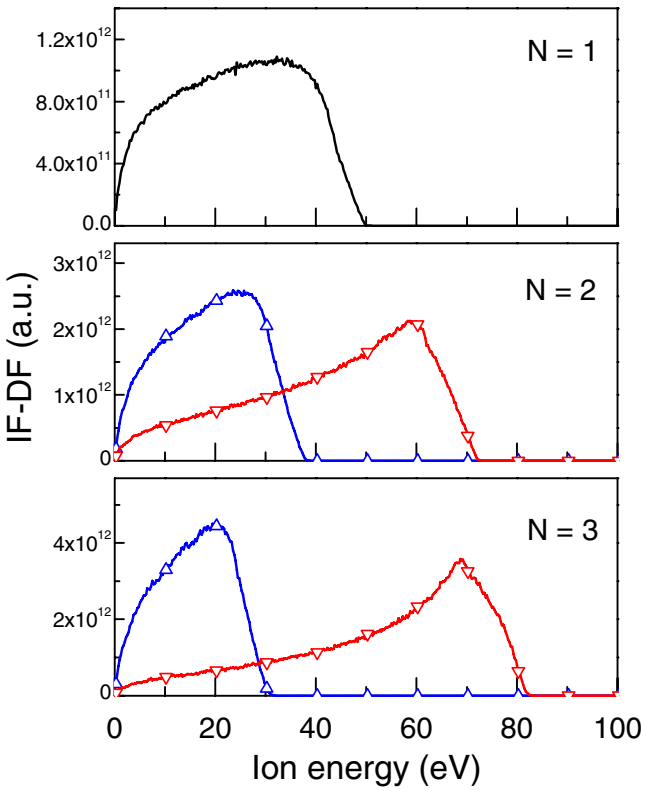


**Figure 15.** Simulated IF-DFs (including ions impacting on the surface at all angles) on the grounded electrode for the $H_3^+$ ion for one, two and three harmonics.

a different sheath potential, observed in [20] is degraded in the present work due to the relatively high pressure and, consequently, high collision frequency. Similar observations were made for the $H_2^+$ and $H^+$ ions. These considerations are consistent with the simulation of Ar discharges shown in figure 14 of [8].

## 5. Summary and conclusions

A combined computational–experimental study was performed of a geometrically symmetric capacitively coupled plasma sustained by tailored voltage waveforms in hydrogen. A multispecies hybrid simulation based on particle-in-cell with Monte Carlo collisions (PIC-MCC) for charged species, coupled to a transport and reaction fluid model for neutral species was employed. Experimental plasma diagnostics included electron density, ion flux on the electrodes, dc self-bias, and ion flux-distribution functions (IF-DFs) for three individual ions ($H^+$, $H_2^+$, $H_3^+$).

The applied voltage waveform was the sum of up to three harmonics. Two cases were considered, namely 'peaks' and 'valleys' waveforms. Under these conditions, $H^+$, $H_2^+$, and $H_3^+$ ions bombarding the electrodes exhibited markedly different IF-DFs due to their differences in mass and collisionality in the sheath. The plasma discharge was electrically asymmetric, and a dc self-bias developed, for all but the sinusoidal waveform. This was due to the temporal asymmetry of the applied voltage, giving rise to two different sheath voltages at the powered and grounded electrode. The electron number density, ion flux and absolute value of the dc self-bias all increased with the number of harmonics. The maximum and average ion bombardment energy on the grounded electrode increased with the number of harmonics for the 'valleys' waveforms, while it decreased for the 'peaks' waveforms. Simulation predictions of electron density, dc self-bias, ion bombardment energy, ion flux and IF-DFs for $H_3^+$, $H_2^+$ and $H^+$ were generally in reasonably good agreement with measurements.

This work sets the basis for the development of complex voltage waveforms powering RF capacitive discharges, using hydrogen-diluted feeds, aimed at reducing substrate damage and optimizing ion-induced surface reactions to grow films with desired properties over large areas using PECVD.

## Acknowledgments

PD and DJE acknowledge financial support by the Department of Energy, Office of Fusion Energy Science, contract DE-SC0001939, and the National Science Foundation grant CMMI 1030620. SL acknowledges partial support from MIUR (PRIN 2010ERFKXL_007). JPB and TL acknowledge support by the Agence Nationale de le Recherche (CANASTA Project No ANR-10-HABISOL-002).

## References

[1] Lieberman M A and Lichtenberg A J 2005 *Principles of Plasma Discharges and Materials Processing* 2nd edn (Hoboken, NJ: Wiley)
[2] Czarnetzki U, Schulze J, Schüngel E and Donkó Z 2011 *Plasma Sources Sci. Technol.* **20** 024010
Donkó Z, Schulze J, Heil B G and Czarnetzki U 2009 *J. Phys. D: Appl. Phys.* **42** 025205
[3] Wang S-B and Wendt A E 2000 *J. Appl. Phys.* **88** 643
[4] Johnson E V, Verbeke T, Vanel J-C and Booth J-P 2010 *J. Phys. D: Appl. Phys.* **43** 412001
[5] Lafleur T, Delattre P A, Johnson E V and Booth J P 2012 *Appl. Phys. Lett.* **101** 124104
[6] Lafleur T and Booth J P 2012 *J. Phys. D: Appl. Phys.* **45** 395203
[7] Lafleur T, Boswell R W and Booth J P 2012 *Appl. Phys. Lett.* **100** 194101
[8] Delattre P A, Lafleur T, Johnson E and Booth J P 2013 *J. Phys. D: Appl. Phys.* **46** 235201
[9] Schulze J, Derzsi A and Donkó Z 2011 *Plasma Sources Sci. Technol.* **20** 045008
[10] Zhang Q-Z, Jiang W, Hou L-J and Wang Y-N 2011 *J. Appl. Phys.* **109** 013308
[11] Schüngel E, Zhang Q-Z, Iwashita S, Schulze J, Hou L-J, Wang Y-N and Czarnetzki U 2011 *J. Phys. D: Appl. Phys.* **44** 285205
[12] Schüngel E, Mohr S, Iwashita S, Schulze J and Czarnetzki U 2013 *J. Phys. D: Appl. Phys.* **46** 175205
[13] Mohr S, Schüngel E, Schulze J and Czarnetzki U 2013 *J. Phys. D: Appl. Phys.* **46** 435201
[14] Schüngel E, Mohr S, Schulze J, Czarnetzki U and Kushner M J 2014 *Plasma Sources Sci. Technol.* **23** 015001
[15] Hrunski D *et al* 2013 *Vacuum* **87** 114
[16] Bruneau B, Wang J, Dornstetter J-C and Johnson E V 2014 *J. Appl. Phys.* **115** 084901
[17] Longo S and Diomede P 2009 *Plasma Process. Polym.* **6** 370
[18] Diomede P, Capitelli M and Longo S 2005 *Plasma Sources Sci. Technol.* **14** 459

[19] Panarese A, Diomede P and Longo S 2013 *Plasma Sources Sci. Technol.* **22** 045017
[20] Diomede P, Longo S, Economou D J and Capitelli M 2012 *J. Phys. D: Appl. Phys.* **45** 175204
[21] Simko T, Martisovits V, Bretagne J and Gousset G 1997 *Phys. Rev.* E **56** 5908
[22] Phelps A V 1990 *J. Phys. Chem. Ref. Data* **19** 653
[23] Longo S 2006 *Plasma Sources Sci. Technol.* **15** S181
[24] Birdsall C K and Langdon A B 1985 *Plasma Physics via Computer Simulation* (New York: McGraw-Hill)
[25] Patterson M M, Chu H Y and Wendt A E 2007 *Plasma Sources Sci. Technol.* **16** 257
[26] Lafleur T, Delattre P A, Booth J P, Johnson E V and Dine S 2013 *Rev. Sci. Instrum.* **84** 015001
[27] Piejak R B, Godyak V A, Garner R, Alexandrovich B M and Sternberg N 2004 *J. Appl. Phys.* **95** 3785
[28] Hamers E A G, van Sark W G J H M, Bezemer J, Goedheer W J and van der Weg W F 1998 *Int. J. Mass Spectrom. Ion Process.* **173** 91
[29] O'Connell D, Zorat R, Ellingboe A R and Turner M M 2007 *Phys. Plasmas* **14** 103510
[30] Lafleur T, Chabert P, Turner M M and Booth J-P 2013 *Plasma Sources Sci. Technol.* **22** 065013
[31] Heil B G, Czarnetzki U, Brinkmann R P and Mussenbrock T 2008 *J. Phys. D: Appl. Phys.* **41** 165202
[32] Wild C and Koidl P 1989 *Appl. Phys. Lett.* **54** 505
[33] Wild C and Koidl P 1991 *J. Appl. Phys.* **69** 2909